

Metal-rim-connected inductive coupler for smartwatch applications

ISSN 1755-4535
 Received on 25th February 2020
 Revised 27th June 2020
 Accepted on 14th July 2020
 E-First on 21st September 2020
 doi: 10.1049/iet-pel.2020.0208
 www.ietdl.org

Jia-Qi Zhu^{1,2}, Yong-Ling Ban¹, Yiming Zhang², Zhengchao Yan^{2,3}, Rui-Min Xu¹, Chunting Chris Mi² ✉

¹School of Electronic Engineering, University of Electronic Science and Technology of China, No. 2006 Xiyuan Avenue, Chengdu, Sichuan, People's Republic of China

²Department of Electrical and Computer Engineering, San Diego State University, 5500 Campanile Drive, San Diego, CA, USA

³School of Marine Science and Technology, Northwestern Polytechnical University, 127 West Youyi Road, Xi'an, People's Republic of China

✉ E-mail: mi@ieee.org

Abstract: A metal-rim-connected inductive coupler with series-*n*-one compensation topology is proposed for smartwatch applications. By cross-connecting the receiving coil to the metal rim with a 1 mm slot, the direction of the induced current on the metal rim is transformed to be the same as the current flowing on the receiving coil, leading to a strong magnetic coupling between the transmitting coil and receiving coil. Considering the space limitation in the smartwatch, non-compensation components are needed inside the smartwatch and only a series capacitance is integrated on the transmitter side. A prototype of the proposed inductive coupler has been built and the wireless power transfer through metal rim has been validated via experiment. The experimental results show that the prototype achieves 5 W output power with 87.4% coil-to-coil efficiency.

1 Introduction

Wireless power transfer (WPT) is a fast developing technology that utilises electromagnetic field to transfer power wirelessly [1]. Inductive power transfer (IPT) and capacitive power transfer are two primary wireless charging methods for consumer electronics, utilising magnetic field and electric field, respectively [2–7]. With cordless, user-friendly and environmentally friendly features, IPT has now become a suitable and popular way for consumer electronics charging [8]. Specifically for smartwatch, achieving IPT can remove the external charging port, leading to better user experience, such as waterproof, dustproof and robustness. Therefore, achieving IPT in a smartwatch is a significant research area.

Until now, few researches have been adopted in smartwatch wireless charging area. As reported in [9], a smartwatch strap wireless charging system was demonstrated with 1.4 W output power of 30% dc–dc power transfer efficiency. By removing the receiving components of the wireless charging system from the mainbody to the strap of the smartwatch, the size, EMI and heat regarding the receiving coils were reduced in the mainbody of smartwatch. However, the strap of the smartwatch will be frequently bent and folded in daily use, leading to inevitable damage and impact on the receiving coil. Besides, the material of strap is constrained to be non-metallic and cannot be replaced by other customised straps without the embedded receiving system. Hence, integrating the receiving components of the IPT system into the mainbody of smartwatch is a good alternative. A method to achieve near field communication for fully enclosed metallic-framed wearable devices was proposed in [10]. However, based on our study in Section 3.1, the method cannot enhance the coupling

coefficient for the smartwatch with metal rim, indicating that the method is not applicable to smartwatch WPT with metal rim.

In consideration of aesthetic appearance and mechanical strength, metal rims are integrated into most of the smartwatches, such as Apple watch series 5, Samsung Galaxy Watch Active 2 and Huawei Watch GT 2, whose metal rims are fabricated by stainless steel, as shown in Fig. 1 [11]. Conventionally, the metal rim is not used for WPT and the receiving coil (Rx coil) must be located at the very bottom of the smartwatch to ensure that no metallic components (digital cameras, lithium-ion battery, GPS/WIFI antennas etc.) are embedded between the transmitting coil (Tx coil) and Rx coil. Also, the back cover is required to be fabricated by non-metallic material to achieve inductive coupling. If the prerequisite and already-existing metal rim is utilised and inductive power is transferred through side way, the vertical position of Rx coil will be much more flexible and the inductive coupler is easier to be integrated with other components. Besides, the back cover of the smartwatch can be fabricated by metallic material to enhance robustness and save cost. With regard to WPT through metal barrier, several studies have been adopted. An IPT system was proposed in [12] to achieve power transfer for metal cover smartphones. Combined with a camera hole and flash hole, a T-slot is required to achieve wireless power transfer (WPT) through the metal cover. Here, these big clearance zones cannot be provided by the metal rim of smartwatch so that it is not suitable for a smartwatch with a metal rim. To realise WPT through a metal barrier, a combined capacitive and inductive coupler was studied in [13]. It does achieve WPT through metal plates, however, the size of the transmitting plates, Rx coil, the primary and secondary compensating circuits are too large to be embedded in a wireless charging system for smartwatch applications.

In this paper, an inductive coupler with series-*n*-one (SN) compensation topology is proposed for smartwatch applications. To achieve inductive coupling through the metal rim, a narrow 1 mm slot is cut on the metal rim. By crossly connecting the Rx coil and the metal rim, the induced current flowing on the metal rim is transformed to be the same as the current flowing on the Rx coil, so the metal rim is converted from a metallic block to be part of the Rx coil, leading to the increase of coupling coefficient. Since the space inside of the smartwatch is limited, SN compensation topology is introduced to make the wireless charging system compact. It is noteworthy that the novelty of this paper is the



Fig. 1 Model of popular smartwatch in the market with metal rim

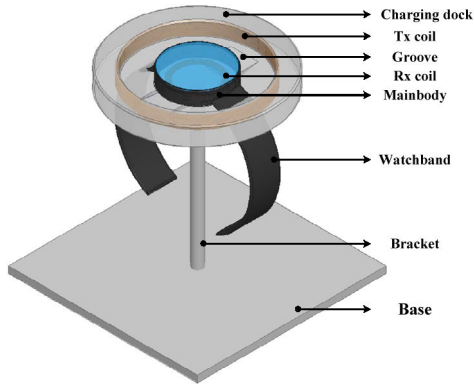


Fig. 2 Schematic diagram of the whole wireless charging system

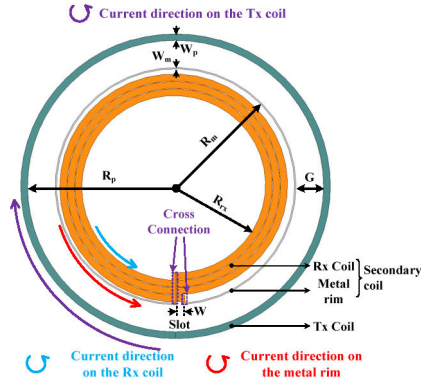


Fig. 3 Plan view of the proposed inductive coupler

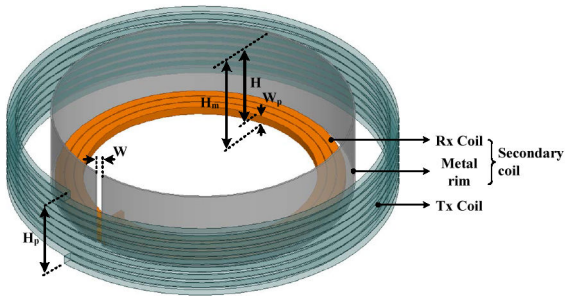


Fig. 4 Side view of the proposed inductive coupler

proposed inductive coupler for smartwatch that enhances the inductive coupling and transfers power through metal rim rather than the SN topology.

2 Structure of the smartwatch inductive coupler

The schematic diagram of the whole wireless charging system is shown in Fig. 2. At the bottom of the stack are the base and bracket, which support the charging dock. On the top of the stack is the charging plate, consisting of the inverter and Tx coil. The main body of smartwatch is placed in the middle of charging plate and the Rx coil is integrated to achieve wireless power transfer. For convenient consideration, two shallow grooves are embedded on the charging plates for people to place and take the smartwatch. By introducing two holes on the charging plate for the watchbands to go through, the watchband does not need to be removed before charging the smartwatch.

The plan view of the inductive coupler for the smartwatch is shown in Fig. 3. An air gap lies between the Tx coil and the metal rim, which is annotated as G . A 1 mm narrow slot is loaded on the metal rim and the Rx coil is in cross-connection with the metal rim by two jumper lines. As a whole, the Rx coil together with the metal rim is defined as the secondary coil.

The side view of the proposed inductive coupler for the smartwatch is shown in Fig. 4. As regard of the Tx coil, it is vertically wound with eight turns to achieve a strong inductive

Table 1 Dimensions of the proposed coupler

Parameter	Value	Parameter	Value
R_p	21.5 mm	R_m	17.3 mm
R_{rx}	12.8 mm	N_p	8
N_{rx}	3	W_p	1 mm
W_m	0.2 mm	W_{rx}	1 mm
G	4 mm	W	1 mm
H	9 mm	H_p	9.8 mm
H_m	10 mm	—	—

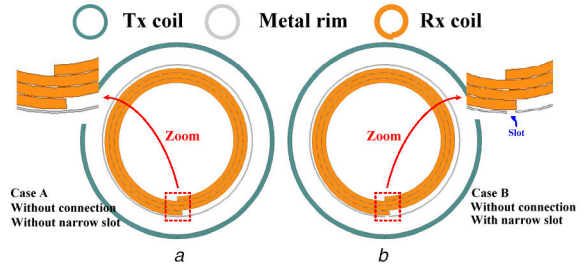


Fig. 5 Five cases regarding the Rx coil and the metal rim (a) Case A, (b) Case B

coupling with the secondary coil. To save space of the smartwatch, the winding number of the Rx coil is only 3 with no compensation circuits. In practical consideration, the height of the metal rim is set as 10 mm. Here, the Rx coil locates at the bottom of the proposed coupler and it is on the same level as the bottom of the Tx coil.

For better view, the detailed dimension of the coupler is listed in Table 1, where R_p represents the inner radius of the Tx coil, R_m is the inner radius of the metal rim, R_{rx} is the inner radius of the Rx coil, N_p is the turns number of the Tx coil, N_{rx} is the turns number of the Rx coil, W_p is the thickness of the Tx coil, W_m is the thickness of the metal rim, W_{rx} is the thickness of the Rx coil, G is the gap between the Tx coil and secondary coil, W is the width of the slot cut on the metal rim, H is the vertical position of the Rx coil, H_p is the height of the Tx coil and H_m is the height of the metal rim. Here, the Tx and Rx coils are closely winding in the experiment and the radius change per turn for the coils are set to 1.1 mm in simulation.

3 Design of the smartwatch inductive coupler

3.1 Design of the secondary coil

In this section, ANSYS Maxwell is applied to analyse and design the inductive coupler for the smartwatch. Since the skin depth of the 1 MHz operating frequency is 65 μm , the AWG 44 Litz-wire of 300 strands is used to build the Tx and Rx coils considering the current rating.

To achieve strong coupling between the Tx coil and the secondary coil, five cases have been studied with the structure shown in Figs. 5 and 6. The corresponding simulation results are listed in Table 2. Here, only cases are varied and other parameters like gap G remains the same for Table 2. In case A, the Rx coil is not in conjunction with the unbroken metal rim and the resultant coupling coefficient is relatively poor, only 0.042. Compared with case A, a 1 mm slot is embedded on the metal rim for case B. Obviously, coupling coefficient k_{ps} between the Tx coil and the secondary coil has been significantly increased. Besides, the inductance L_p of the Tx coil is increased, leading to a smaller compensation capacitance C_1 . With regard to case C, the Rx coil is in same connection with the 1 mm slot loaded metal rim. In this way of connection, the current on the metal rim is in opposite direction with the current flowing in the Rx coil and the magnetic field generated by the Rx coil will be weakened by the metal rim. Therefore, the coupling coefficient k_{ps} and the inductance L_s of the secondary coil are decreased comparing with case B. Regarding case D, by cross-connecting the Rx coil with the metal rim, the

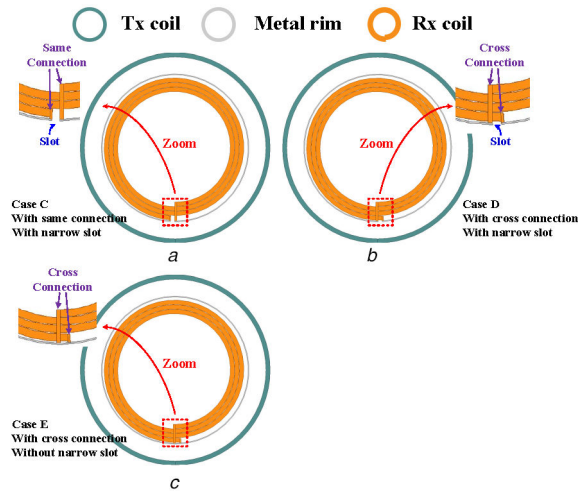


Fig. 6 Five cases regarding the Rx coil and the metal rim
(a) Case C, (b) Case D, (c) Case E

Table 2 Simulation results of the inductive coupler in different cases

Parameters	Scheme				
	Case A	Case B	Case C	Case D	Case E
k_{ps}	0.042	0.395	0.241	0.467	0.041
L_p , μH	2.50	3.81	3.81	3.83	2.52
L_s , μH	0.238	0.397	0.276	0.603	0.244

Table 3 Simulation results of the inductive coupler with different slot width

Parameters	Slot width W , mm					
	0	0.1	0.5	1	1.5	2.0
k_{ps}	0.041	0.468	0.467	0.466	0.466	0.466
L_p , μH	2.52	3.83	3.83	3.83	3.83	3.83
L_s , μH	0.244	0.601	0.603	0.603	0.605	0.606

metal rim becomes part of the Rx coil and the direction of the current induced on the metal rim is transformed to be the same with the current flowing on the Rx coil, leading to a further increased inductive coupling between the Tx coil and the secondary coil comparing with case B. In this circumstance, the loss of the secondary coil is essentially the same as a regular coil so that the secondary coil is modelled by an equivalent series inductance L_s and resistance R_s to calculate the loss. Here, it is noteworthy that the coupling coefficient k_{ps} will be as low as 0.04 if the Rx coil is in cross-connection with an unbroken metal rim, as indicated in case E. In conclusion, case D is selected to construct the secondary coil.

Since the metal rim nearly wraps the LED display and the main body of smartwatch, the overall height of smartwatch is approximately equal to the height of the metal rim plus the height of the sensors part. According to [11], the overall heights of Apple watch series 5, Samsung Galaxy Watch Active 2 and Huawei Watch GT 2 are 10.7, 10.9 and 10.7 mm, respectively. Considering that the sensors part only takes a small portion of the overall height, the height H of the metal rim is practical and reasonable to be set as 10 mm. Also, if H changes from 6 to 14 mm, the parameters of the proposed inductive coupler (k_{ps} , L_p , L_s) change little (not shown here for brevity). That is because the metal rim serves as a winding of the secondary coil. Thus, the height H of the metal rim in the proposed inductive coupler can be varied to accommodate different smartwatches.

3.2 Impact of the slot width

As a slot is integrated on the metal rim, the width of the slot becomes a vital parameter to study. As indicated in Table 3, the width W of the slot is increased from 0 to 2 mm with an increment

of 0.5 mm and a single value at 0.1 mm. It is noteworthy that other parameters including gap G are fixed in the study of width W . Obviously, the parameters of the inductive coupler do not change with the variation of the slot width, even at the extremely small slot width of 0.1 mm. However, the coupling coefficient k_{ps} , inductance of the Tx coil and the secondary coil will dramatically decrease without the slot integrated (0 mm slot width). Here, the width of 0.1 mm is used to compare with the case where there is no slot cut. In other words, the 0.1 mm slot width represents an extremely small slot cut condition and it can be varied. For example, if the slot width is 0.01 or 0.2 mm, the parameters (k_{ps} , L_p and L_s) will not change as compared with the condition of 0.1 mm slot width. Considering the significant enhancement on performance, the slot cut is necessary to be implemented, even if the slot will relatively reduce the mechanical strength of the smartwatch. Also, the slot width should be as small as possible, which helps to maintain the mechanical strength. The slot width is finally set as 1 mm due to the constraints of manual craft in the lab.

3.3 Vertical position of the Rx coil

Together with the Rx coil, various components with different functions are needed to be embedded in the smartwatch. Accommodating with other components, the vertical position of the Rx coil will vary in different smartwatches so that the Rx coil should be flexible in vertical position variation. As shown in Fig. 7, the parameter H represents the vertical position of the Rx coil. With the increase of H from 1 to 9 mm (Rx coil locates from top to bottom of the smartwatch), the parameters (k_{ps} , L_p and L_s) of the inductive coupler do not change. For brevity, the simulation results are not shown here.

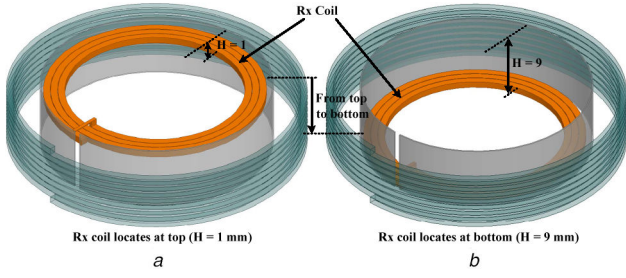


Fig. 7 Vertical position variation of the Rx coil
(a) $H = 1$ mm, (b) $H = 9$ mm

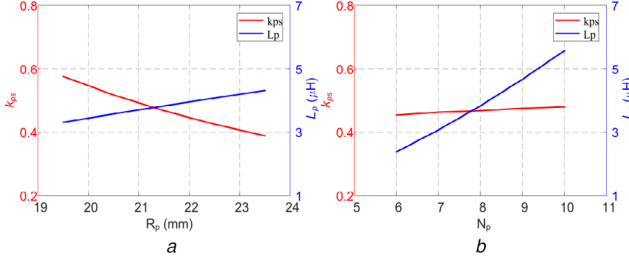


Fig. 8 Coupling coefficient k_{ps} and inductance L_p regarding
(a) Radius R_p , (b) Turn number N_p

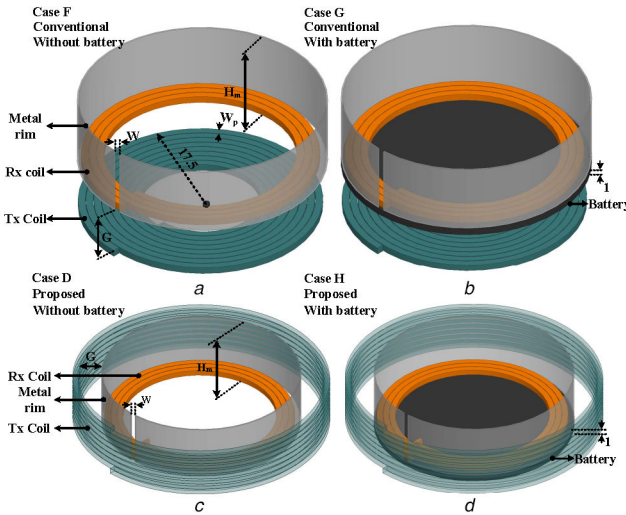


Fig. 9 Layout of the conventional coupler and proposed coupler
(a) Conventional coupler with battery, (b) Conventional coupler without battery, (c) Proposed coupler with battery, (d) Proposed coupler without battery

Table 4 Simulated parameter comparison with conventional inductive coupler

Parameter	Conventional		Proposed	
	Case F	Case G	Case D	Case H
k_{ps}	0.417	0.008	0.467	0.229

3.4 Design of the Tx coil

As shown in Fig. 8a, the coupling coefficient k_{ps} will decrease with the increase of Tx coil radius (R_p). However, with the increase of R_p , the inductance of Tx coil will become bigger, leading to a smaller compensation capacitor (C_1). Therefore, considering both the coupling coefficient and compensation capacitor, the radius of Tx coil is set as 21.5 mm. Here, the Tx coil can be wound vertically or horizontally. If the Tx coil is wound horizontally, the coupling coefficient will be 0.32, which is smaller than the vertical winding of 0.46. Besides, the coupling coefficient will vary bigger by changing the vertical position of the Rx coil comparing with vertically winding. Therefore, the Tx coil is wound vertically to achieve stronger and stable coupling. As indicated in Fig. 8b, the

coupling coefficient is nearly unchanged with the variation of the Tx coil turn number (N_p). The inductance of the Tx coil is increased with the increase of N_p , resulting in a smaller compensation capacitor C_1 . Since the Tx coil is vertically wound, the height of the charging dock in Fig. 2 is dependent on the turn number (N_p). Thus, considering both the compensation capacitor and the volume of the charging dock, the turn number of Tx coil is set as 8.

3.5 Comparison with the conventional inductive coupler

Conventionally, the Rx coil usually locates at the bottom of the smartwatch to avoid metallic components (digital cameras, lithium-ion battery, GPS/WIFI antennas etc.) embedded between the Tx coil and Rx coil. To achieve wireless charging, magnetic wireless charger is usually utilised, and the Tx coil is placed under the smartwatch, such as Apple Watch Series and Samsung Galaxy Watch Active 2 [11]. For comparison purpose, four cases are proposed, as shown in Fig. 9. In case F, the Tx coil is located under the smartwatch and the Rx coil is not in conjunction with the metal rim. For fair comparison, the 1 mm slot is reserved on the metal rim. Also, the gap (G) between the Tx and Rx coil is set to be the same with the proposed coupler. To make the space occupation of the conventional coupler to be comparable with the proposed coupler, the radius of the Tx coil in case F is set to be the same with the metal rim. Here, the coupling-coefficient-reduction property with an integrated metallic layer for the conventional coupler that discussed in the next paragraph will be the same regardless of the radius of the Tx coil. Compared with case F, a metallic layer of 17.5 mm radius is integrated between the Tx coil and Rx coil for case G, which may represent a battery or bottom metal cover in practical. It is noteworthy that the radius of the metallic layer may vary for different components in the smartwatch. As for case D, it represents the proposed inductive coupler. With regard to case H, it indicates the proposed inductive coupler with the same embedded metallic layer as case G.

The corresponding coupling coefficients for different cases are shown in Table 4, where the coupling coefficient of case D is slightly higher than case F, indicating that the proposed coupler has little advantage over the conventional coupler with direct comparison. However, a metallic layer may exist at the bottom of the smartwatch, which represents the bottom metal cover or battery pack. In this case, the coupling coefficient decreases dramatically from 0.417 (case F) to 0.008 (case G) for the conventional coupler. As for the proposed coupler, the coupling coefficient decreases from 0.467 (case D) to 0.229 (case H) after integrating the metallic layer, indicating that the proposed inductive coupler can still achieve good performance with metallic components on the bottom of the smartwatch. That is because the proposed coupler converts the already existing metal rim from a metal barrier to part of the secondary coil and the power can transfer through the side of smartwatch.

In conclusion, the proposed inductive coupler achieves much better performance than conventional coupler with integrated metallic components on the bottom of smartwatch. Besides, the back cover of the smartwatch can be fabricated by metallic material to enhance mechanical strength and durability with the proposed inductive coupler. According to Section 3.3, unlike conventional coupler, the Rx coil of the inductive coupler does not have to be placed at the very bottom of the smartwatch to avoid embedded metallic components between the Tx and Rx coil. The flexibility of the Rx coil makes the proposed inductive coupler easy to be accommodating with other components like antennas and batteries inside the smartwatch.

4 Working principle of the resonant inductive coupler

In consideration of compact space in the smartwatch, an SN compensation topology is applied. Integrating the designed inductive coupler, the circuit topology of the proposed IPT system for smartwatch is shown in Fig. 10. A full-bridge inverter is

applied to generate AC source power. Only a series capacitor C_1 is served for compensation at the transmitter side.

The fundamental harmonics approximation (FHA) method is used to analyse the working principle of the circuit topology, as shown in Fig. 11 [14]. It is noteworthy that the secondary coil is analysed by an equivalent model composing of a series inductance L_s and resistance R_s to calculate the loss. The inductance L_s in Fig. 11 represents the whole secondary coil, including both the metal rim and the Rx coil. High-order harmonics of the output square wave are neglected so that the output of the inverter is approximately equivalent to a sinusoidal source. The angular frequency is defined as ω .

According to [15], to achieve constant voltage output, C_1 should be derived as

$$C_1 = \frac{1}{\omega^2 L_p (1 - k_{ps}^2)}. \quad (1)$$

The magnetic couplings between the Tx coil and the secondary coil are represented by current-controlled voltage sources. By applying Kirchhoff's voltage law to the primary side and secondary side, (2) can be derived as

$$\begin{cases} (j\omega L_p + \frac{1}{j\omega C_1} + R_p)I_1 + j\omega M_{ps}I_2 = V_1 \\ j\omega M_{ps}I_1 + (j\omega L_s + R_s + R_L)I_2 = 0 \end{cases}. \quad (2)$$

In (2), R_p and R_s represent the resistances of the Tx coil and secondary coil, respectively. With quality factors Q_p and Q_s of the Tx coil and secondary coil, the resistances can be calculated as $R_p = \omega L_p / Q_p$ and $R_s = \omega L_s / Q_s$.

With (1) and (2), the input current I_1 and output current I_2 are derived as (see (3)). With current I_1 and I_2 calculated using (3), the output power P_{out} and efficiency η are calculated as (4) and (5), respectively

$$P_{out} = I_2^2 R_L \quad (4)$$

$$\eta = \frac{1}{1 + (R_p [(\omega L_s)^2 + (R_L + (\omega L_s / Q_s))^2] / \omega^2 M^2 R_L) + (R_s / R_L)} \quad (5)$$

In case that the metal rim is touched during the charging process, the voltage on the metal rim should be within safety range. According to [16, 17], the safe RMS voltage on the metal rim is required to be lower than 8.35 V.

To calculate the voltage on the metal rim, the secondary coil is split into the metal rim and Rx coil for analysis, as indicated in Fig. 12. The inductance relationship between the metal rim (L_{rim}), Rx coil (L_{rx}) and the secondary coil (L_s) is expressed as

$$L_s = L_{rx} + L_{rim} + 2M_{rx,rim}. \quad (6)$$

Here, the worst case occurs when people touch across the two edges of the narrow slot. Since the metal rim is a small single winding coil, the resistance of it can be neglected and the maximum voltage V_{rim} on the metal rim is calculated as

$$V_{rim} = j\omega M_{p,rim}I_1 + j\omega M_{rx,rim}I_2 + j\omega L_{rim}I_2. \quad (7)$$

The mutual inductance $M_{p,rim}$ between the Tx coil and metal rim, mutual inductance $M_{rx,rim}$ between the Rx coil and metal rim and L_{rim} are simulated as 232, 80.8 and 41.3 nH, respectively. With a 1 MHz working frequency, Q_p of 113, Q_s of 52, 5 Ω load resistance

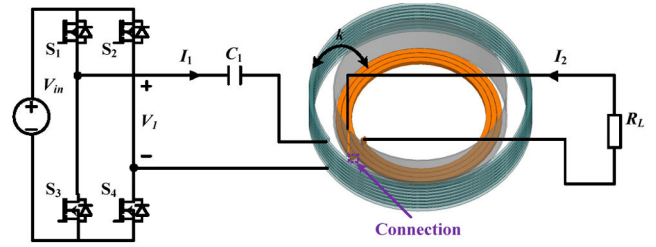


Fig. 10 Schematic circuit diagram of the proposed metal-rim-connected IPT system

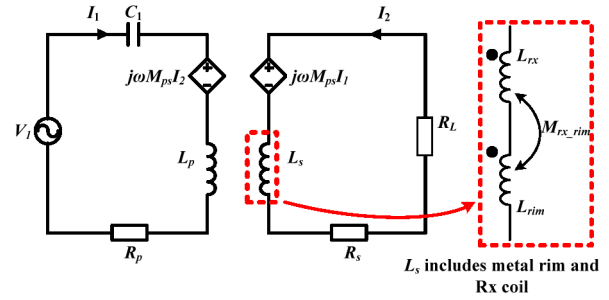


Fig. 11 Simplified FHA circuit model of the proposed metal-rim-connected IPT system

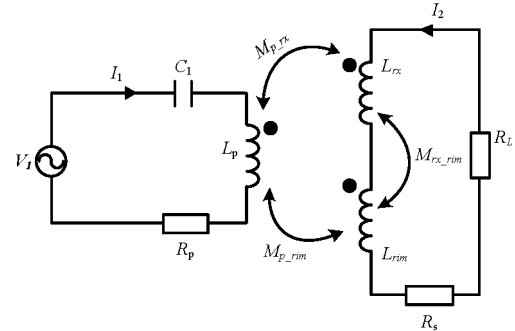


Fig. 12 Circuit model of the proposed IPT system to calculate the voltage on the metal rim

R_L and 5 W output power, the RMS voltage on the metal rim is calculated as 2.9 V, which is far below the required safe voltage (8.35 V). Here, Q_p and Q_s are substituted by measured values for calculation. In the actual design process, it needs to be pointed out that the quality factors are estimated by experience at the preliminary design stage to evaluate the currents, output power and coil-to-coil efficiency.

5 Experiment and calculation

The prototype of the proposed inductive coupler for smartwatch was fabricated and tested, as shown in Fig. 13. A quarter dollar was placed beside the proposed coupler as a reference. The Tx coil and Rx coil were both fabricated by AWG 44 Litz-wire with 300 strands in consideration of operating frequency and current rating. A segment of PVC tube was utilised to fill in the 4 mm air layer between the Tx coil and the metal rim. To successfully conduct the experiment, the metal rim was constructed by gluing a copper sheet with 10 mm height on the inner side of the PVC tube. The gluing gap of the metal sheet represents the 1 mm width slot loaded on the metal rim. To realise cross-connection with the Rx coil, one edge of the slot was connected to the load resistance R_L and the other edge was in conjunction with the Rx coil.

$$\begin{cases} I_1 = \frac{V_1}{((\omega M)^2 / (j\omega L_s + R_L + (\omega L_s / Q_s))) + j\omega L_p + (1 / j\omega C_p) + (\omega L_p / Q_p)} \\ I_2 = \frac{j\omega M V_1}{((\omega M)^2 / (j\omega L_s + R_L + (\omega L_s / Q_s))) + j\omega L_p + (1 / j\omega C_p) + (\omega L_p / Q_p) (j\omega L_s + R_L + (\omega L_s / Q_s))} \end{cases} \quad (3)$$

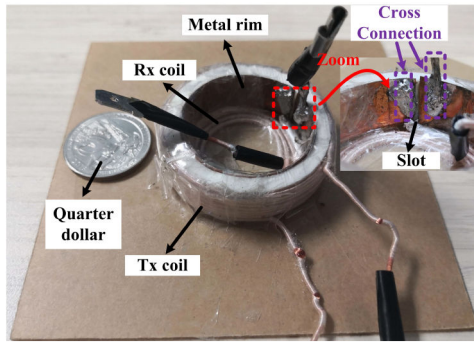


Fig. 13 Fabricated prototype of the proposed metal-rim-connected inductive coupler

Table 5 Experimental parameters of the proposed inductive coupler

Parameter	Value	Parameter	Value
L_p	3.85 μH	Q_p	113
L_s	0.62 μH	R_L	5 Ω
Q_s	52	k_{ps} : proposed	0.46
k_{ps} : case A	0.05	k_{ps} : case B	0.37

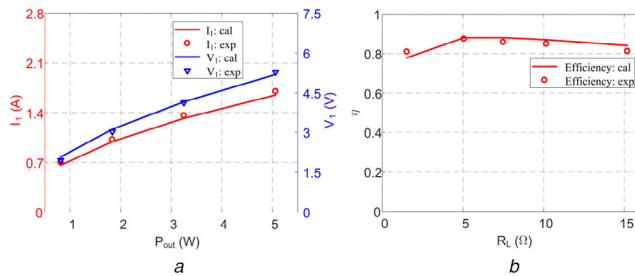


Fig. 14 Calculated and measured (a) Input current I_1 and voltage V_1 , (b) Efficiencies at different output power P_{out}

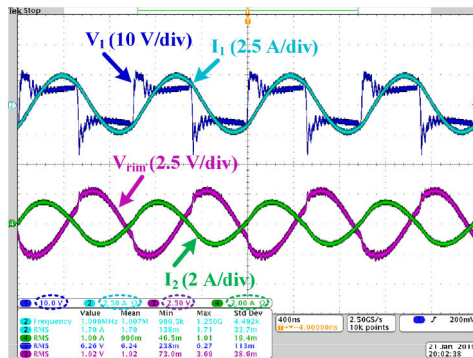


Fig. 15 Experimental waveforms of the proposed metal-rim-connected inductive coupler

The corresponding experimental parameters of the fabricated inductive coupler are listed in Table 5. Compared with case A and case B from Fig. 5, the proposed inductive coupler (case D) significantly enhances the coupling coefficient from 0.05 to 0.46 by crossly connecting the Rx coil to the edge of the narrow slot. The working frequency was set at 1 MHz to obtain suitable capacitance C_1 . According to (1), the compensated capacitance C_1 was chosen as 8 nF integrating with the compensated capacitance C_1 , the inductive coupler was connected to an inverter for AC source power. It is noteworthy that the inverter was only used to verify the characteristic of the proposed inductive coupler together with the SN compensation topology. As the output power P_{out} varies from 0.8 to 5 W (output current I_2 from 0.4 to 1 A with an increment of 0.2 A), the calculated and measured input voltage V_1 and input current I_1 of the inductive coupler are shown in Fig. 14a.

Since the inductance of the secondary coil is relatively small, the inductance (230 nH) of connecting wire and load resistance is taken into consideration for calculation. With the variation of load resistance from 1.5 to 15 Ω , the corresponding calculated and measured coil-to-coil efficiencies η are shown in Fig. 14b. With 5 Ω R_L , the coil-to-coil efficiency (AC-to-AC) is measured to be 87.4%.

With 5 W output power (I_2 equals to 1 A), the experimental waveforms were shown in Fig. 15, where the corresponding scales of the waveforms are denoted with the labels and marked by dotted circle. Zero voltage switching had been achieved and the voltage across the slot of the metal rim is validated to be only 1.92 V with 5 W output power, which is far below the safety voltage (8.35 V). Here, the calculated input impedance at the DC-AC converter is $2.11 + j2.33$, leading to a phase difference of 47.8° between the input voltage V_1 and input current I_1 . The experimental phase difference corresponds well with the calculated result. As indicated in Fig. 15, the time difference between V_1 and I_1 is about 130 ns, leading to a 46.8° phase difference at 1 MHz. This inductive impedance characteristic is inherent with the SN topology. Therefore, the SN compensation topology is suitable for consumer electronics, such as smartwatch applications because of the required limited space and small power level.

Since the compensated capacitor C_1 is derived for constant voltage output, the proposed topology is robust against load variation to a certain extent. However, if the gap between the Tx coil and secondary coil varies in practice, the coupling coefficient k_{ps} will be changed, leading to the variation of output voltage. Consequently, the efficiency of power transmission will be reduced in long transfer distances due to weakly-coupled coils, and in short transfer distances, as a result of frequency splitting phenomenon [18]. To make the system robust against variations in distance and load transfer, closed-loop control strategies are necessary and presented in literature for some applications such as biomedical implanted devices [19]. Proposing a closed-loop control scheme for smartwatch applications will be one of our research directions in future research.

6 Conclusion

In this paper, a novel inductive coupler is proposed for metal rim smartwatches. At the transmitter side, the eight turns vertical-winding Tx coil is in series with an 8 nF compensation capacitor. At the receiver side, namely inside the smartwatch, the three turns horizontal winding Rx coil (12.8 mm inner radius) is integrated with no compensation components. By cross-connecting the Rx coil with the 1 mm narrow slot loaded metal rim, the metal rim is converted from a metal barrier to part of the secondary coil, which significantly increase the coupling coefficient from 0.05 to 0.46 and wireless power transfer through metal rim is thus achieved. With 5 W output power, 87.4% coil-to-coil efficiency is achieved. In the coupler, the slot width and vertical position of the Rx coil do not influence the performance. Besides, the utilisation of the already-existing metal rim makes the inductive coupler flexible and easy to be integrated with other components inside the smartwatch. Therefore, the proposed metal-rim-connected inductive coupler is a good candidate for smartwatch applications.

7 References

- [1] Li, S., Mi, C.C.: 'Wireless power transfer for electric vehicle applications', *IEEE Trans. Emerg. Sel. Top. Power Electron.*, 2015, **3**, (1), pp. 4–17
- [2] Hui, S.Y.R., Ho, W.C.: 'A new generation of universal contactless battery charging platform for portable consumer electronic equipment', *IEEE Trans. Power Electron.*, 2005, **20**, (3), pp. 620–627
- [3] Covic, G.A., Boys, J.T.: 'Inductive power transfer', *Proc. IEEE*, 2013, **101**, (6), pp. 1276–1289
- [4] Zhong, W.X., Liu, X., Hui, S.Y.R.: 'A novel single-layer winding array and receiver coil structure for contactless battery charging systems with free-positioning and localized charging features', *IEEE Trans. Ind. Electron.*, 2011, **58**, (9), pp. 4136–4144
- [5] Dai, J., Ludois, D.: 'A survey of wireless power transfer and a critical comparison of inductive and capacitive coupling for small gap applications', *IEEE Trans. Power Electron.*, 2015, **30**, (11), pp. 6017–6029

- [6] Liu, C., Hu, A.P., Wang, B., *et al.*: 'A capacitively coupled contactless matrix charging platform with soft switched transformer control', *IEEE Trans. Ind. Electron.*, 2013, **60**, (1), pp. 249–260
- [7] Zhu, J.Q., Ban, Y.L., Zhang, Y., *et al.*: 'A novel capacitive coupler array with free-positioning feature for Mobile tablet applications', *IEEE Trans. Power Electron.*, 2019, **34**, (7), pp. 6014–6019
- [8] Hui, S.Y.: 'Planar wireless charging technology for portable electronics products and Qi', *Proc. IEEE*, 2013, **101**, (6), pp. 1290–1301
- [9] Jeong, S., Kim, D.H., Song, J., *et al.*: 'Smartwatch strap wireless power transfer system with flexible PCB coil and shielding material', *IEEE Trans. Ind. Electron.*, 2019, **66**, (5), pp. 4054–4064
- [10] Choi, J., Lim, S., Hong, W.: 'Efficient NFC coil antennas for fully enclosed metallic-framed wearable devices', *IET Microw. Antennas Propag.*, 2020, **14**, (3), pp. 211–214
- [11] 'Apple watch series 5, Samsung Galaxy Watch Active 2, and Huawei Watch GT 2', Available at: <https://www.gsmarena.com/>, accessed May 6
- [12] Jeong, N.S., Carbolante, F.: 'Wireless charging of a metal body device', *IEEE Trans. Microw. Theory Tech.*, 2020, **65**, (4), pp. 1077–1086
- [13] Zhou, W., Su, Y., Huang, L., *et al.*: 'Wireless power transfer across metal barrier by combined capacitive and inductive coupling', *IEEE Trans. Ind. Electron.*, 2019, **66**, (5), pp. 4031–4041
- [14] Safaei, A., Woronowicz, K.: 'Time-domain analysis of voltage-driven series-series compensated inductive power transfer topology', *IEEE Trans. Power Electron.*, 2017, **32**, (7), pp. 4981–5003
- [15] Zhang, Y., Kan, T., Yan, Z., *et al.*: 'Modeling and analysis of series-parallel compensation for wireless power transfer systems with a strong coupling', *IEEE Trans. Power Electron.*, 2019, **34**, (2), pp. 1209–1215
- [16] IEEE International Committee on Electromagnetic Safety: 'IEEE standard for safety levels with respect to human exposure to radio frequency electromagnetic fields, 3 kHz to 300 GHz', 2005
- [17] International Electrotechnical Commission: 'Method of measurement of touch current and protective conductor current', 1999
- [18] Niu, W.Q., Chu, J.X., Gu, W., *et al.*: 'Exact analysis of frequency splitting phenomena of contactless power transfer systems', *IET Trans. Circuits Syst. I, Regul. Pap.*, 2013, **60**, (6), pp. 1670–1677
- [19] Nasr, F., Madani, S.M., Niroomand, M.: 'Dual-objective control strategy for maximum power and efficiency point tracking in wirelessly powered biomedical implanted devices', *IET Microw. Antennas Propag.*, 2020, **14**, (1), pp. 36–44